

Photon counting statistics of superconducting single-photon detectors made of a three-layer WSi film

I. N. Florya

Moscow State Pedagogical University, ul. Malaya Pirogovskaya 1, str. 1, Moscow 119991, Russia

Yu. P. Korneeva

Moscow State Pedagogical University, ul. Malaya Pirogovskaya 1, str. 1, Moscow 119991, Russia and Institute for Physics of Microstructures, Russian Academy of Sciences, Nizhnyi Novgorod 603950, Russia

M. Yu. Mikhailov^{a)}

B. I. Verkin Institute for Low-Temperature Physics and Engineering, National Academy of Sciences of Ukraine, pr. Nauki 47, Kharkiv 61103, Ukraine

A. Yu. Devizenko

National Technical University "Kharkiv Polytechnical Institute," ul. Kirpicheva 2, Kharkiv 61002, Ukraine

A. A. Korneev^{a)} and G. N. Goltsman

Moscow State Pedagogical University, ul. Malaya Pirogovskaya 1, str. 1, Moscow 119991, Russia and A. N. Tikhonov Moscow Institute of Electronics and Mathematics, National Research University "Higher School of Economics," ul. Myasnitskaya 20, Moscow 101000, Russia

(Submitted October 27, 2017)

Fiz. Nizk. Temp. **44**, 292–297 (March 2018)

Superconducting nanowire single-photon detectors (SNSPD) are used in quantum optics when record-breaking time resolution, high speed, and exceptionally low levels of dark counts (false readings) are required. Their detection efficiency is limited, however, by the absorption coefficient of the ultrathin superconducting film for the detected radiation. One possible way of increasing the detector absorption without limiting its broadband response is to make a detector in the form of several vertically stacked layers and connect them in parallel. For the first time we have studied single-photon detection in a multilayer structure consisting of three superconducting layers of amorphous tungsten silicide (WSi) separated by thin layers of amorphous silicon. Two operating modes of the detector are illustrated: an avalanche regime and an arm-trigger regime. A shift in these modes occurs at currents of ~ 0.5 – 0.6 times the critical current of the detector. *Published by AIP Publishing.* <https://doi.org/10.1063/1.5024539>

1. Introduction

The operating principle of superconducting nanowire single-photon detectors (SNSPD) was demonstrated in 2001.¹ Today, detectors of this type are used in quantum optics and quantum cryptography where they perform better than single-photon avalanche diodes in the 1310–1550 nm telecommunications band.² Their quantum efficiency, i.e., the probability of detecting a photon, is limited, however, by the absorption coefficient of the superconducting film used in the SNSPD and is usually less than 30%. In order to increase the absorption, a detector is built into an optical cavity similar to a Fabry-Perot etalon. A record quantum efficiency of 93% has been obtained with this approach at 1550 nm.³ Of course, when a cavity is used the detector bandwidth and sensitivity are reduced.

An alternative approach for increasing the absorption without loss of bandwidth is to make a detector in the form of several superconducting layers mounted above one another.⁴ A three-dimensional structure has been built⁵ with 2 superconducting meanders of WSi stacked on top of one another and electrically connected in parallel. Because of the

mutually orthogonal positions of the meanders, at the same time the polarization dependence of the detection efficiency was also reduced.

Two approaches were combined in Ref. 6: a two-layer SNSPD of WSi was integrated into an optical cavity consisting of multilayer dielectric mirrors mounted on the side of the substrate and a transparent coating on the vacuum side. This detector had a detection efficiency of $87.1 \pm 1.3\%$ for 1450–1640 nm.

It is evident that simply increasing the number of superconducting meanders mounted on top of one another without using a cavity can also lead to increased quantum efficiency. At the same time, this should increase the critical superconducting current and bias current for this kind of detector and, thereby, lead to an increase in the voltage pulse amplitude when a photon is detected. When the meanders are connected in parallel in a multilayer SNSPD, however, two operating modes, similar to those observed in single SNSPD with parallel meanders,^{7–9} are to be expected.

In the first mode, if the current in each section of a single-layer detector is sufficiently close to the critical

current, one section switches into the normal state when a photon is absorbed, and the current from that section will be redistributed along the remaining $N-1$ sections, after which the current in them exceeds the critical value. This induces an avalanche switching of all the sections into the resistive state. This mechanism is referred to as the avalanche regime and these detectors are referred to as superconducting nanowire avalanche photodetectors (SNAP).⁹

The second mode occurs at lower bias currents. As in the avalanche regime, here the current from a section that has absorbed a photon is redistributed among the other sections. If, however, the bias currents of the sections are sufficiently low before absorption of a photon, then after redistribution of the currents they do not reach the critical value, the remaining sections do not enter the resistive state, and a voltage pulse is not produced in the detector. In the section that absorbed the photon, the current does not recover even after the section returns to the superconducting state. After several cycles of photon absorption, however, a distribution of the currents is established such that after regular absorption of a photon the current redistribution nevertheless leads to an avalanche switching of all the sections. In this mode, which is referred to as the arm-trigger regime, the detector responds only to a sequence of two or more absorbed photons.⁹

In this paper, for the first time we study a multilayer-SNAP detector in which three superconducting layers are mounted vertically above one another and investigate the conditions for the transition from avalanche to trigger detection.

2. Sample preparation technique

We made multi-layer ML-SNAP detectors consisting of three layers of superconducting amorphous WSi film with a thickness of 34 Å separated by an insulating Si barrier of thickness 51 Å (Fig. 1). The substrates were 2500-Å-thick polished silicon slabs with thermal oxide SiO₂. All the layers were deposited by dc magnetron sputtering using two sources with tungsten and silicon targets. Deposition of the first WSi layer was followed by deposition of a 60-Å-thick sublayer of amorphous silicon, which improves the superconducting properties and ensures better uniformity of the next amorphous superconducting film.¹⁰ After deposition of the third superconducting layer, a 30-Å-thick layer of silicon was deposited for protection from oxidation. During deposition, the substrate was at room temperature. The thickness of

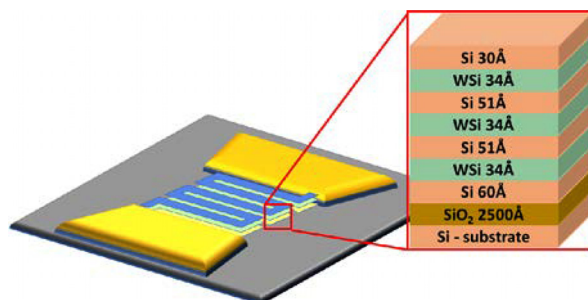


Fig. 1. A sketch of the transverse cross section of a multilayer SNSPD with each superconducting WSi layer separated by an insulating Si layer. All the superconducting layers are connected in parallel and output to a pair of contacts.

the films and insulating barriers between them in the multilayer composite was determined by small-angle x-ray reflectometry following deposition. Transmission electron microscopy data show that the superconducting and insulating layers have an amorphous structure. The nominal atomic proportion W:Si of the elements in the superconducting layer is 75:25, which ensures a maximum critical temperature.

In the limit of thick silicon spacers, our multilayer sample can be treated as a set of independent superconducting WSi layers connected in parallel. But Si spacers that are too thick may affect the accuracy of the required detector topology during dry etching processing. With thinner silicon spacers the critical temperature of the multilayer superconductor increases due to enhanced interlayer coupling via Josephson tunneling. Previous studies^{11,12} have shown that multilayer S/I composites with an Si-barrier behave as two-dimensional uncoupled layers for barrier thickness $d_{\text{Si}} > 40\text{--}50$ Å. Thus, for fabricating ML-SNAP detectors we chose a silicon spacer thickness of 51 Å. The critical temperature of the fabricated three-layer detectors was $T_c = 3.5 \pm 0.1$ K. The resistivity of the ML-SNAP, $\rho = 194 \mu\Omega \cdot \text{cm}$, was determined from the resistance of a square film R_{\square} and its thickness d . The resulting value of R_{\square} is a factor of 3 smaller than for a single WSi layer with a thickness of 34 Å.

A nanostrip in the form of a meander was produced by electron-beam lithography followed by reactive ion etching in an SF₆ plasma. The meanders were made with sizes of 10×10 or $7 \times 7 \mu\text{m}$. The width of the strip in different samples was 73–128 nm and the range of distances between strips was 72–127 nm. Cr/Cu electrical contacts were made by electron-beam evaporation and structured by photolithography.

3. Experimental setup

All the measurements were made at a temperature of 1.7 K. The detector was mounted on a holder in a measurement cell in an evacuated cryogenic insert located in a Dewar flask containing liquid helium. The detector chip was connected by ultrasonic welding to a coplanar line and adjusted relative to a single-mode SMF-28 fiber in the holder. The coplanar line was connected by a coaxial-coplanar adapter to a coaxial line. A Mini Circuits ZFBT-4R2GW+ bias adapter was used for dc bias of the detector. The signal from the sample was amplified by a cascade of broadband (0.1–1000 MHz) Mini Circuits ZFL-1000 LN+ amplifiers with a combined gain of 46 dB and fed to a Tektronix DPO-70404C oscilloscope (4 GHz bandwidth, 25 G samples/s) and an Agilent 53131 pulse counter to measure the detection efficiency. The radiation source was a 1550 nm cw laser.

The quantum efficiency, i.e., the probability of detecting a photon, was defined as the ratio of the number of photon counts to the number of photons incident on the sample. The number of photons, in turn, was determined from the radiant power and the attenuation.

4. Results and discussion

26 samples were prepared. All the fabricated samples had a critical current in the 3–10 μA range. To choose the

best, we measured the detection efficiency at a wavelength of 1550 nm.

For a study of the operating mode we selected several typical samples with a high detection efficiency. Here we present the results for one of them (with a size of $10 \times 10 \mu\text{m}$, strip width of 111 nm, and a distance of 89 nm between the strips). At the working temperature of 1.7 K the critical current for this sample was $8 \mu\text{A}$. The detection efficiency η and dark count rate of this detector are plotted in Fig. 2(a) as functions of the bias current. The maximum value of η was $\sim 30\%$, or somewhat lower than the theoretical value for the absorption coefficient of the multilayer structure studied here [Fig. 2(b)]. Note that saturation is not observed at currents close to I_c in the plot of η as a function of current. We believe this indicates that the sample is either insufficiently cooled or there are imperfections in the superconducting strips. In addition, the overall reduction in detection efficiency may also be related to an unequal distribution of the current between the strips. In fact, if one of the strips has a smaller bias current, then the detection efficiency in it will be lower, thereby reducing the detection efficiency of the structure as a whole.

We then studied the statistics of the dependence of the number of photon counts on the number of incident photons. It can be shown¹ for SNSPD with a low photon flux that if the detector receives single photons, the dependence of the number of photon counts per unit time will be proportional to the first power of the photon flux incident on the detector. If, on the other hand, the detector requires simultaneous absorption of two photons in order to work, the number of photon counts will be proportional to the square of the photon flux; if three photons are required, then it is proportional to the cube, etc.

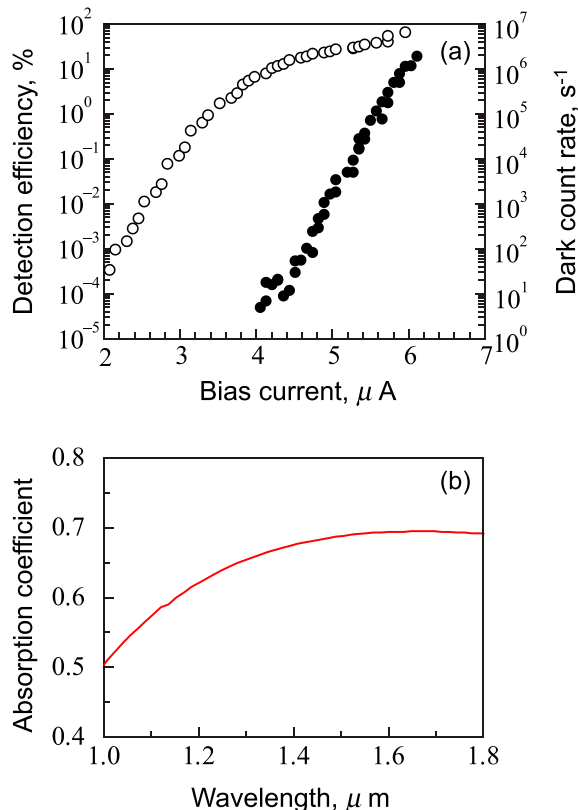


Fig. 2. (a) Detection efficiency at 1550 nm (○) and dark count rate (●) as functions of bias current. (b) Calculated absorption coefficient of the multilayer structure of the samples studied here.

This follows from the fact that for a Poisson distribution with an average number of photons $\nu \ll 1$ within a time interval τ , the probability of n photons within this time interval simplifies to $\rho_n = \nu^n/n!$. Strictly speaking, the time τ should be taken to be the time for formation of a hot spot, i.e., a region with suppressed superconductivity at the site where a photon is absorbed. Since this time is not known precisely, however, it is possible to take the photoresponse time of the detector as a stricter condition on τ . In addition, photons incident on widely separated segments of the detector have no effect whatever on one another. Thus, we have to examine how many photons are incident over a time τ on an area whose size is on the order of that of a hot spot. Estimates show that this region is smaller than the width of a strip, so it is appropriate to use the width of an entire superconducting strip instead of the width of the hot spot as the stricter condition. Even under these conditions, the photon fluxes used in our experiment were low. Figure 3 shows plots of the number of photon counts as a function of photon flux measured for different detector bias currents: 4, 5, and 6 μA . It can be seen that for all bias currents the photon count rate is proportional to the first power of the photon flux.

It can, however, be shown that dependences of this kind will be observed in the avalanche and arm-trigger regimes. In order to distinguish one regime from the other, we used an analysis of the statistics of the time intervals between two successive photon counts which can be used to determine the number of successively absorbed photons required for a transition of the detector into a resistive state in the arm-trigger regime.

Using the Tektronix DPO-70404C digital oscilloscope we recorded a trace of duration 10 ms with a time resolution of 800 ps. This time resolution made it possible to obtain at least one point in the leading edge and another 2–3 points in the trailing edge in a recorded pulse (Fig. 4). As a result, we obtained a set of times t_i and corresponding instantaneous voltages U_i . Then the times t_{iA} corresponding to the appearance of the photon counts were determined by a program. We took the voltage excess above a threshold value, which is easily determined since the amplitude of the voltage pulse U_{iA} is well above the amplitude of the noise, as a criterion. Using the set of values of t_{iA} we found the time intervals between all successive photon counts $\Delta t_i = t_{i+1} - t_i$. We then constructed

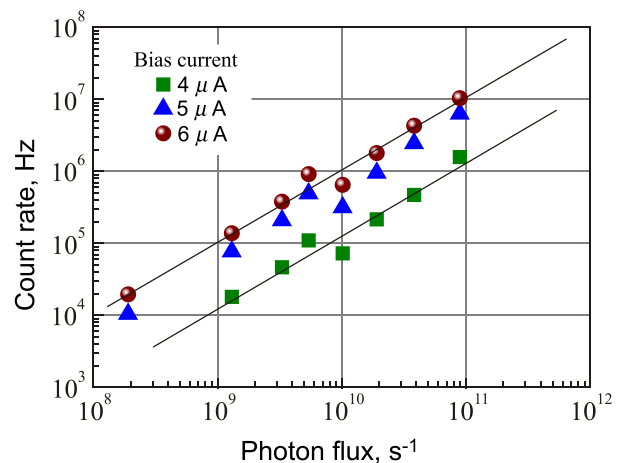


Fig. 3. The number of photon counts as a function of photon flux at 1550 nm for three sample currents. The straight lines correspond to direct proportionality between the number of photon counts and the photon flux.

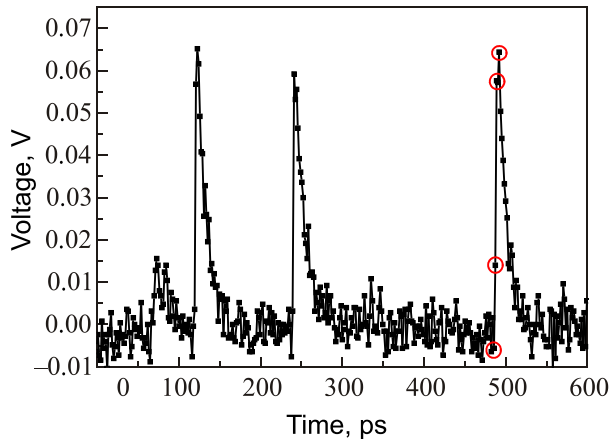


Fig. 4. Part of an oscilloscope trace obtained with a Tektronix DPO-70404C digital oscilloscope. The duration of the full trace was 10 ms and the time resolution was 800 ps.

a histogram of the distribution of these time intervals normalized to the number of time intervals and their width.

If the photons are independent and obey a Poisson distribution, then the probability that n photons will be incident on the detector over a time t is equal to $(\nu t)^n e^{-\nu t} / n!$, where ν is the average number of photons incident on the detector per unit time. Let the first count be observed at time $t = 0$. The probability of a second count in the time between t and $t + dt$ is the product of the probabilities of having exactly one photon in the interval from t to $t + dt$ and of having $n-1$ photons in the interval from 0 to t . The probability of the first event is νdt and of the second, $(\nu t)^{n-1} e^{-\nu t} / (n-1)!$; their product is equal to $\nu dt (\nu t)^{n-1} e^{-\nu t} / (n-1)!$. We obtain the distribution of the time intervals between photons, i.e., the probability density of the time for a second photon count to occur by dividing the product of these probabilities by dt

$$\rho(t) = \nu (\nu t)^{n-1} e^{-\nu t} / (n-1)! \quad (1)$$

The photon counting statistics were measured for powers of 0.94, 2.77, and 7.3 pW at 1550 nm, which correspond to 7.3×10^6 , 2.2×10^7 , and 5.7×10^7 incident photons per second. Figure 5 shows plots of the count rate as a function

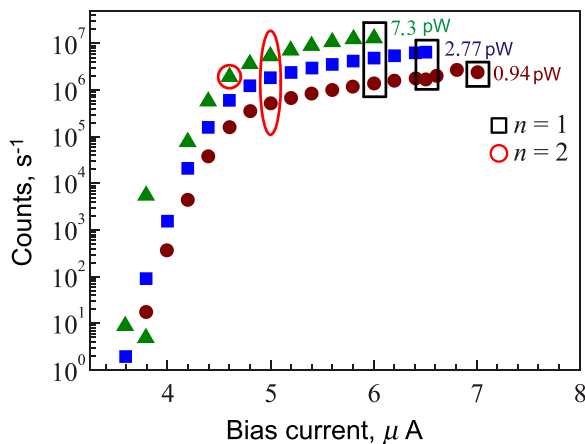


Fig. 5. The dependence of count rate on bias current. The incident power was varied from 0.94 to 7.3 pW. The rectangles and ovals indicate the points at which the photon count statistics was studied. The points enclosed in black rectangles were observed in the avalanche regime ($n=1$) and the points enclosed in red ovals, in the arm-trigger regime ($n=2$).

of bias current. The rectangle and ovals indicate the points at which the counting statistics were studied in accordance with Eq. (1). Typical histograms of the distributions are shown in Fig. 6. The histogram in Fig. 6(a) was measured at the point $I_b = 6 \mu\text{A}$ with a power of 2.77 pW. The histogram shows that a single photon ($n=1$) is sufficient to switch the detector into the resistive state. Similar histograms were constructed at the points with bias currents of 6, 6.5, and 7 μA for all the powers studied here. The histogram of Fig. 6(b) was obtained at the point $I_b = 5 \mu\text{A}$ with a power of 2.77 pW. The best approximation to this histogram with Eq. (1) was obtained for $n=2$, i.e., such that 2 photons are required to produce a response. Since the test samples consisted of only three superconducting layers, it was not possible to observe the statistical distributions for $n > 2$.

For all the powers used here, the arm-trigger regime with $n=2$ was observed for currents below $0.52I_c$ and the avalanche regime ($n=1$) began to be observed stably at currents greater than $0.58I_c$. For currents between $0.52I_c$ and $0.58I_c$, a mixed mechanism related to the transition from $n=1$ to $n=2$ was observed. Similar behavior was observed for all the test samples.

If it is assumed that the strips in all three layers are the same, the currents between them will also be distributed the same way, and it is assumed that when a photon is absorbed, the current in a strip falls almost to zero, then for a sample with three strips the transition from the arm-trigger to the

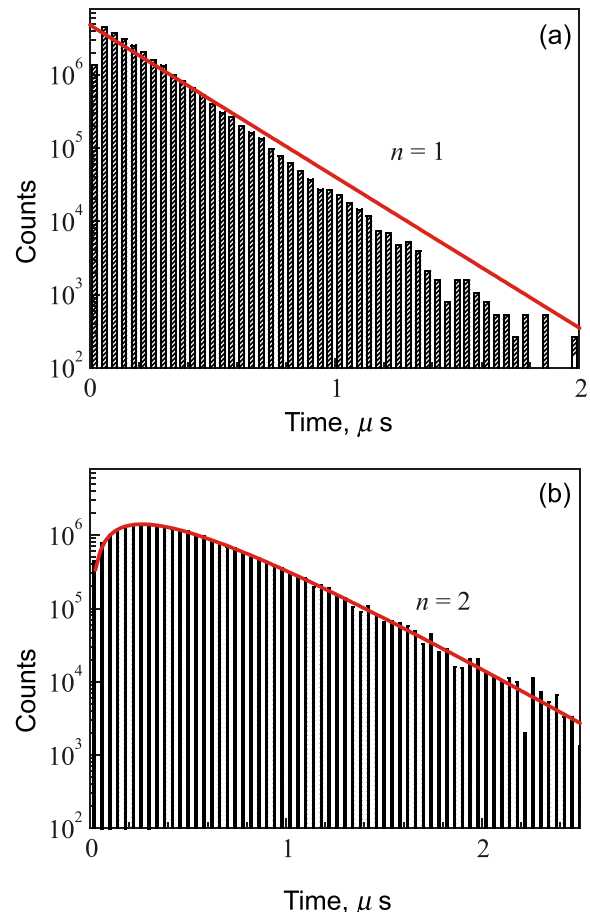


Fig. 6. Typical histograms of the distribution of the time intervals between two successive photon counts corresponding to (a) $n=1$ (avalanche regime) and (b) $n=2$ (arm-trigger regime). The smooth red curves are approximations according to Eq. (1).

avalanche regime should occur at a current of $I_c/2$. In our experiments, the regime shift was observed at slightly higher currents, which indicates a nonuniform distribution of the currents between strips or that the current does not go to zero in a strip that has detected a photon.

5. Conclusion

We have demonstrated the feasibility of making a superconducting single-photon detector in the form of a three-layer WSi/Si structure. The typical quantum efficiencies were about 30%, which is lower than the expected absorption coefficient, apparently because of defects in fabricating the strips and an insufficiently low working temperature.

In a study of the statistics of the time intervals between two successive photon counts, we have shown that the detector works in both avalanche and arm-trigger regimes. The shift in operating regimes occurs at currents of $\sim 0.5I_c$ – $0.6I_c$, apparently because of a nonuniform distribution of the currents between the superconducting strips in different layers or because the current in a strip does not fall to zero when a photon is detected.

This work was supported by technical task No. 88 for scientific research at the National Research University “Higher School of Economics,” Grant No. 14.V25.31.0007 from the Ministry of Education and Science of Russia, and the work of G. N. Goltsman was supported by task No. 3.7328.2017/VU of the Ministry of Education and Science of Russia.

^{a)}Electronic addresses: mikhailov@ilt.kharkov.ua and akorneev@rplab.ru

-
- ¹G. N. Gol'tsman, O. Okunev, G. Chulkova, A. Lipatov, A. Semenov, K. Smirnov, B. Voronov, and A. Dzardanov, *Appl. Phys. Lett.* **79**, 705 (2001).
- ²C. M. Natarajan, M. G. Tanner, and R. H. Hadfield, *Supercond. Sci. Technol.* **25**, 063001 (2012).
- ³F. Marsili, V. B. Verma, J. A. Stern, S. Harrington, A. E. Lita, T. Gerrits, I. Vayshenker, B. Baek, M. D. Shaw, R. P. Mirin, and S. W. Nam, *Nat. Photonics* **7**, 210 (2013).
- ⁴A. Jafari Salim, A. Eftekharian, and A. Hamed Majedi, *J. Appl. Phys.* **115**, 054514 (2014).
- ⁵V. B. Verma, F. Marsili, S. Harrington, A. E. Lita, R. P. Mirin, and S. W. Nam, *Appl. Phys. Lett.* **101**, 251114 (2012).
- ⁶S. Krapick, M. Hesselberg, V. B. Verma, I. Vayshenker, S. W. Nam, and R. P. Mirin, preprint [arXiv:1706.00004](https://arxiv.org/abs/1706.00004) (2017).
- ⁷M. Ejrnaes, R. Cristiano, O. Quaranta, S. Pagano, A. Gaggero, F. Mattioli, R. Leoni, B. Voronov, and G. Gol'tsman, *Appl. Phys. Lett.* **91**, 262509 (2007).
- ⁸F. Marsili, F. Najafi, C. Herder, and K. K. Berggren, *Appl. Phys. Lett.* **98**, 093507 (2011).
- ⁹F. Marsili, F. Najafi, E. Dauler, F. Bellei, X. Hu, M. Csete, R. J. Molnar, and K. K. Berggren, *Nano Lett.* **11**, 2048 (2011).
- ¹⁰J. M. Graybeal and M. R. Beasley, *Phys. Rev. B* **29**, 4167 (1984).
- ¹¹E. Rosseel, M. Baert, K. Temst, C. Potter, V. V. Moshchalkov, Y. Bruynseraede, P. Lobotka, I. Vavra, R. Senderak, and M. Jergel, *Physica C* **225**, 262 (1994).
- ¹²M. Yu. Mikhailov, O. I. Yuzepovich, A. S. Pokhila, Yu. V. Bomze, N. Ya. Fogel, I. M. Dmitrenko, S. A. Yulin, A. S. Sidorenko, and O. B. Moldovan, *Fiz. Nizk. Temp.* **25**, 850 (1999) [*Low Temp. Phys.* **25**, 635 (1999)].

Translated by D. H. McNeill